ELSEVIER

Atmospheric Research 52 (1999) 59–75

ATMOSPHERIC RESEARCH

www.elsevier.com/locate/atmos

Effect of crystal size spectrum and crystal shape on stratiform cirrus radiative forcing

Ying Zhang [a,*], Andreas Macke [b], Frank Albers [a]

[a] *Institute for Atmospheric Physics, GKSS Forschungszenterum, Geesthacht 21502, Germany*
[b] *Institute for Maritime Research, Kiel, Germany*

Received 20 May 1998; received in revised form 26 April 1999; accepted 4 May 1999

Abstract

Sensitivities of cirrus cloud radiative forcing as well as solar albedo and infrared emittances to ice crystal size spectrum and ice crystal shape were examined using a coupled cloud-radiation model. The single- and bi-modal crystal size distribution were considered and simulated based on field measurements. Optical parameters of ice crystals shaped as hexagonal columns and random polycrystals (being frequently found in cirrus clouds) were calculated with a ray-tracing method. Both solar and infrared cirrus radiative forcing are influenced by the pattern of crystal size spectra. The net radiative forcing is lower for bi-modal than for single-modal spectra. The solar radiative forcing of cirrus cloud is reduced by nonspherical ice crystals, due to larger albedo effects of nonspherical crystals compared to those of equivalent spherical crystals. Moreover, this reduction in solar radiative forcing by random polycrystals is even larger than that by hexagonal column crystals. The cloud radiative forcing, solar albedo and infrared emittance are changed significantly as the mean crystal size approaches the smaller size end. Furthermore, net cloud radiative forcing is positive in most cirrus cases. Exceptions are cirrus clouds with a large number ($> 10^7$ m^{-3}) of small (mean maximum dimension < 30 μm) ice crystals and cirrus clouds with bi-modal crystal size distribution and large particle size for the second maximum peak. © 1999 Elsevier Science B.V. All rights reserved.

Keywords: Cloud; Radiation; Cirrus; Radiative forcing; Cloud microphysics

1. Introduction

The impact of cirrus clouds on the radiative budget depends on the balance between reflective and absorptive properties of cirrus clouds, which are determined by the cloud

* Corresponding author. E-mail: ying.zhang@gkss.de

0169-8095/99/$ - see front matter © 1999 Elsevier Science B.V. All rights reserved.
PII: S0169-8095(99)00026-5

microphysical, thermal and optical features. Previous research has revealed that cloud microphysical features influence essentially on cloud radiative properties. The work of Kinne and Liou (1989), Mishchenko et al. (1996) and Macke et al. (1998) indicated that the effects of crystal nonsphericity on aldebo of cirrus clouds and cirrus solar radiative transfer are very significant. Small ice particles can produce high cloud albedo and infrared emittance (Stephens et al., 1990; Zhang et al., 1994). To evaluate the radiation budget responding to changes in cloud physical properties, the cloud radiative forcing (CRF) is estimated. CRF is a perturbation of atmospheric radiative balance caused by clouds, calculated as the difference between the disturbed value and that in a cloudless atmosphere. There are several current definitions of radiative forcing (e.g., Stenchikov et al., 1997). In this work, the instantaneous cloud radiative forcing is chosen and defined as the changes in net radiative flux at the top of the atmosphere due to clouds. The change in radiation budget at the top of the atmosphere would cause temperature changes at the surface or in the atmosphere. Therefore, CRF also indicates potential changes in climate due to clouds.

Scattering properties of crystals with nonspherical shapes were simulated by using a ray-tracing method developed by Macke (1993, Macke et al. (1996). They found that the reflectance of ice clouds depends essentially on ice particle shape. Furthermore, previous work by Macke et al. (1996) indicates that the scattering properties of hexagonal column crystals could be representative for those of most column type ice crystals.

Table 1 exhibits several cases of cirrus particle size distribution measured in several projects such as FIRE (The First ISCCP Regional Experiment), ICE (International Cirrus Experiment), EUCREX (European Cloud and Radiation Experiment) and from other field measurements. Although these in situ-measured cirrus particle size distributions vary greatly from case to case, the bi-modal pattern of ice particle size distribution was frequently found in cirrus clouds along with the single-modal pattern. Moreover, in many cases, ice crystal size distributions were found to vary vertically (e.g., Heymsfield and Platt, 1984; Koch, 1996). The crystal size spectra measured at various cloud levels during EUCREX 1994 over the polar seas (Koch, 1996) are shown in Fig. 1. The single-modal size spectra of ice crystals were found near the cloud top and the bi-modal size spectra in the lower portion of the cloud. The second maximum peak in the bi-modal size spectra drifts to larger crystal size at lower cloud layers. Bi-modal ice crystal size spectra in cirrus were also measured during FIRE II by using PMS 2DC probes and an ice particle replicator (Arnott et al., 1994).

The microphysical features of contrail-induced cirrus clouds have been measured and compared with natural cirrus by Gayet et al. (1996). It was found that contrail cirrus are composed of much smaller (quasi-spherically shaped) ice crystals (with a size of about 35 μm) and with a much higher particle concentration (about 800 l^{-1}) than natural

Notes to Table 1:
R_{mini}: crystal size at the minimum concentration trough.
R_{maxi1}: crystal size at the first maximum concentration peak.
R_{maxi2}: crystal size at second maximum concentration peak.
N_{maxi1}: the first maximum in crystal concentration.
N_{maxi2}: the second maximum in crystal concentration.

Table 1
Some of cirrus measurement cases

Investigator (year of publication)	Cloud type	Instruments	Spectrum pattern	Microphysical features
Heymsfield (1975)	cirrus uncinus, cirrostratus		bi-modal, single-modal	range: 20–1100 μm, $R_{maxi2} = 500$ μm
Knollenberg et al. (1982)	stratospheric cirrus anvil	2D grey imaging probe	tri-modal	
Heymsfield and Platt (1984)	cirrus		single-modal, bi-modal	
Mitchell et al. (1996)	all types of cirrus (FIRE II)	ice particle replicator	bi-modal	range: 20–450 μm, $R_{maxi1} = 20$ μm, $R_{mini} = 150$ μm, $R_{maxi2} = 250$–300 μm, $N_{maxi1} = 7\times10^{5}$ m^{-3}, $N_{maxi2} = 5\times10^{2}$ m^{-3}
Arnott et al. (1994)	cirrus (FIRE II)	PMS 2DC, ice particle replicator	bi-modal	$R_{maxi1} = 20$ μm, $R_{mini} = 100$ μm, $R_{maxi2} = 200$–300 μm, $N_{maxi1} = 10^{5}$ m^{-3}, $N_{maxi2} = 10^{3}$ m^{-3}
Koch (1996)	Arctic cirrus (EUCREX)	PMS OAP 2D2-C	single-modal, bi-modal	range: 40–500 μm, $R_{mini} = 100$–200 μm, $R_{maxi1} = 40$ μm, $R_{maxi2} = 100$–300 μm, $N_{maxi1} = 10^{3}$ m^{-3}, $N_{maxi2} = 10^{2}$ m^{-3}
Albers (1991)	jet stream cirrus frontal cirrus (EUCREX)	PMS OAP, Hallet replicator	single-modal, single-modal	more ice water and larger ice crystals are found in frontal cirrus than in jet stream cirrus
Gayet et al. (1996)	contrail cirrus, natural cirrus (ICE)	PMS 2D-C	single-modal, bi-modal	high ice particle number density and small particles are found in contrail cirrus; $R_{maxi2} = 300$–400 μm, $N_{maxi1} = 10^{3}$ m^{-3}, $N_{maxi2} = 10^{1}$ m^{-3}, $R_{mini} = 200$ μm

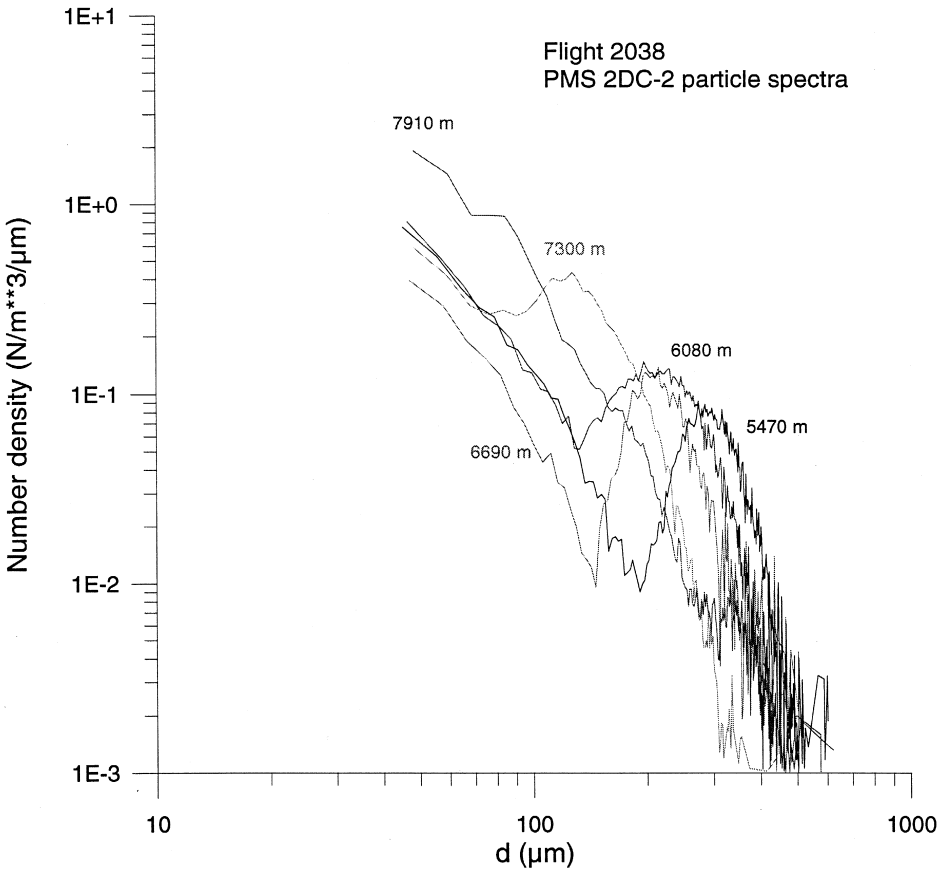

Fig. 1. Bi-modal ice crystal size spectra measured during EUCREX (Koch, 1996). *d* is the diameter of the sphere with equivalent surface area.

cirrus clouds. This kind of high particle concentration in contrail cirrus agrees with the results of Rangno and Hobbs (1983), in which the concentration of small ice particles produced by aircraft was as high as 1000 l^{-1}. The huge number density of very small ice particles in contrail cirrus is also confirmed by Kaercher et al. (1996). Potential impacts of anthropogenic cirrus on the climate were investigated by Sassen (1997).

The measured cirrus physical properties exhibit variety and complexity. The influence of cirrus on the climate depends on the radiative properties of the clouds, which are closely related to the cloud physical properties. The cirrus-radiation parameterizations in some GCMs which describe rather simplified physical features of the clouds are not suitable for the more precise modeling needed in cirrus-radiation and cirrus-climate studies. However, before more sophisticated parameterizations are applied into GCMs for better cirrus-radiation simulations, it is important to know how cirrus radiative properties and cirrus radiative forcing depend on the complex physical properties of clouds.

The purpose of this work is to investigate and recognize the dependence of cirrus cloud radiative forcing and radiative properties on cloud microphysical features. The cloud microphysical features considered were crystal size distribution and crystal shape. Single- and bi-modal crystal size distributions, based on field-measured results, were simulated and their relation to cloud radiative properties and cirrus radiative forcing were investigated. The radiative features of crystals with hexagonal column shapes and random polycrystals calculated by the ray-tracing method and their impact on cirrus radiative forcing were studied and compared with those of spherical crystals.

The model used for the simulation and evaluation of cirrus cloud radiative and microphysical characters is described in Section 2. In Section 3, the sensitivities of cirrus cloud radiative forcing and cloud radiative properties to the crystal size distribution and the shape of ice crystals are evaluated. We discuss the results and make conclusions in the final section.

2. The model

The model used in this work is a coupled cloud microphysical-radiative model. Basically, the cloud microphysical module was developed after the work of Ramaswamy and Detwiler (1986) and Zhang et al. (1989, 1992, 1994); infrared and shortwave radiation modules are based on the two-stream radiative transfer codes of Schmetz and Raschke (1981), Schmetz (1984) and Kerschgens et al. (1978). The vertical domain of the model atmosphere reaches up to 50 km. Explicit parameterization of cloud microphysics characterized by particle size distributions is considered. Physical processes in the cloud module include deposition and sublimation of ice crystals, condensation and evaporation of water droplets, sedimentation of crystals and droplets, advective and vertical transportation of cloud particles by dynamic motions, homogeneous and heterogeneous nucleation of droplets and ice crystals, as well as the interaction (collection) of cloud particles. Single or multiple cloud layers or cells are produced in locations with suitable saturation and temperature. In the radiation module, the spectrum in shortwave radiation between 0.2 and 3.28 μm is divided into 50 intervals, and in longwave radiation between 4 and 400 μm into 37 intervals. Besides absorption and/or scattering of cloud ice crystals, those of water droplets, aerosols and gaseous compounds such as water vapour, ozone and CO_2 are taken into account. The delta-Eddington approximation has been used for scattering calculation. The radiation module is coupled with the cloud microphysical module. Infrared and solar radiation serve as heating/cooling forcing on the growth rate of cloud particles as well as on the temperature field, directly and indirectly to alter the cloud microphysical structure and cloud particle size distribution. In turn, the reproduced cloud microphysical structure has an influence on the radiation fields and on the radiative balance at the top of the atmosphere. The current version of the cloud-radiation model is time-dependent and in one or two dimensions. Resolutions are flexible. The time step is taken separately for the cloud module and the radiation module.

The one-dimensional version of the model described above has been used for calculating the cloud radiative forcing in this work. Iteration is taken to find a particle

size distribution with a given mean size fitting the given value of ice water content (IWC), according to the relationship between IWC and particle number density $n(r)$.

$$\mathrm{IWC} = \int_0^\infty \rho n(r) V(r) \mathrm{d}r, \tag{1}$$

where ρ is the density of ice (taken as 0.91 g cm^{-3}, taken from Fischer, 1989) and $V(r)$ is the volume of a particle with size r.

Crystal shapes of hexagonal columnar monocrystals, polycrystals and spheres were chosen in this work. Optical parameters of hexagonal columns and polycrystals were calculated using a ray-tracing method (Wendling et al., 1979; Rockwitz, 1989; Macke, 1993; Macke et al., 1996). The optical parameters of 'spherical' crystal were calculated using Mie theory for bullet-shaped crystal with an equivalent spherical surface area (Ramaswamy and Detwiler, 1986).

In the parameterization of solar and infrared radiative transfer modules, the idea introduced by Stephens et al. (1990) was used for connecting the crystal size distribution with cloud albedo and emittance.

Two types of crystal size distribution, single- and bi-modal, were considered in this work. A large portion of measured crystal size spectra exhibits a bi-modal character (shown in Table 1), i.e., there are two maximum peaks of particle number density in the size distribution curve. Bi-modal size distribution is considered as the sum of the first maximum peak and second maximum peak sections. The first maximum peak section is assumed to obey an exponential function (Mitchell et al., 1996).

$$n_1(r) = N_1 \exp\left(-\frac{r}{r_{m1}}\right), \tag{2}$$

where N_1 is a coefficient related to the maximum of the size spectrum and $1/r_{\mathrm{m1}}$ is the slope of the size spectrum for the first maximum peak section, respectively. The second maximum peak section is simulated using the gamma distribution function

$$n_2(r) = \frac{N_2}{\Gamma(b)} \left(\frac{b}{r_{m2}}\right)^b r^{b-1} \exp\left(-\frac{b}{r_{m2}} r\right), \tag{3}$$

where b is the shape factor that determines the shape of the distribution. Strictly, N_2 is the total number of particles for the second maximum peak section when the size ranges from 0 to infinity. The mean radius of particles for the second maximum peak section is denoted as r_{m2}, which is generally equivalent to the size at second maximum of the crystal size distribution. The particle size r in Eq. (2) and Eq. (3) is defined by the maximum dimension for all particle types.

As the particle size at the second maximum in the bi-modal size distribution moves towards the small size end, the size distribution becomes a single-modal distribution, which can be parameterized by the gamma distribution function mentioned above. Fig. 2 demonstrates idealized, simulated bi-modal size distributions with change in r_{m2} (100–300 μm) for 10 mg m^{-3} IWC. The second peak moves towards the larger size end as r_{m2} increases. At the same time, the particle size corresponding to the minimum trough between peaks increases, depending on the value and location of both peaks.

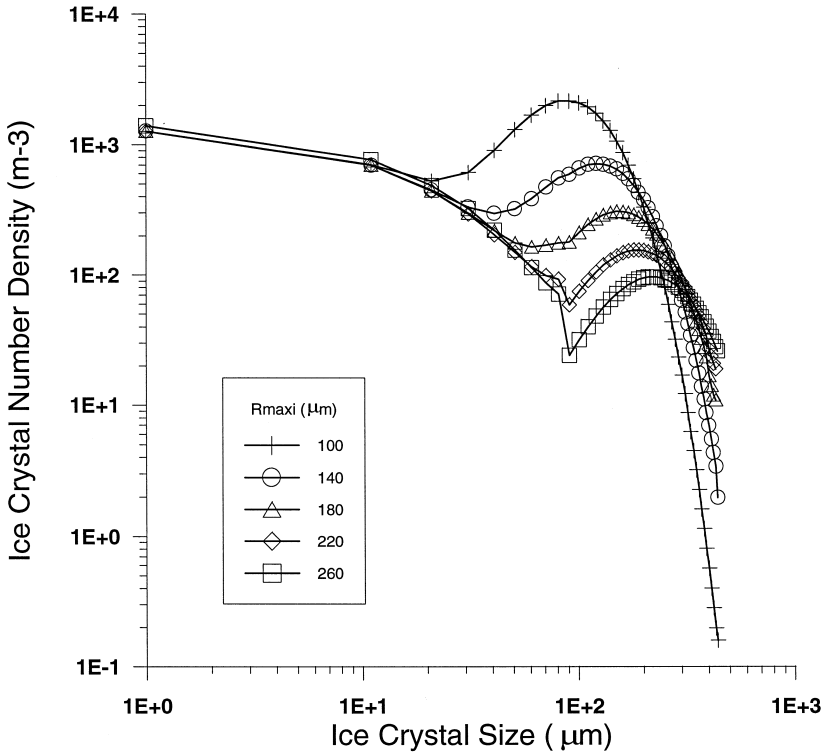

Fig. 2. Simulated bi-modal particle size spectra with the crystal size at the second peak ranging from 100 to 300 μm. The shape factor *b* is 7.

The single modal crystal size distribution was simulated using the gamma distribution function (Eq. (3)).

3. Results

To evaluate the sensitivity of cirrus CRF, it is important that the estimation of CRF is based on the same atmospheric fields and surface albedo, and the same value of IWC. US standard atmospheric model profiles were employed. The near-ground air temperature was taken as 288°K. The solar zenith angle was 60° and surface albedo was 0.13. Cloud was located at an altitude between 10.5 km and 9.5 km (or 8.5 km), and with a thickness of 1 km (or 2 km) and a vertically homogeneous IWC profile. IWC values of 10 mg m^{-3} and 20 mg m^{-3} were chosen. For a given IWC, the shape of cloud particle size distribution can be altered greatly by the changes in mean particle size *r* (or the sizes at the maximum peaks for a bi-modal size spectrum) and particle concentration *N*. The mean value of ice crystal size was changed from 10 μm to 300 μm. The smallest

and largest particle sizes in the size spectrum under consideration were 1 μm and 500 μm, respectively. The shape factor b is taken as 7.

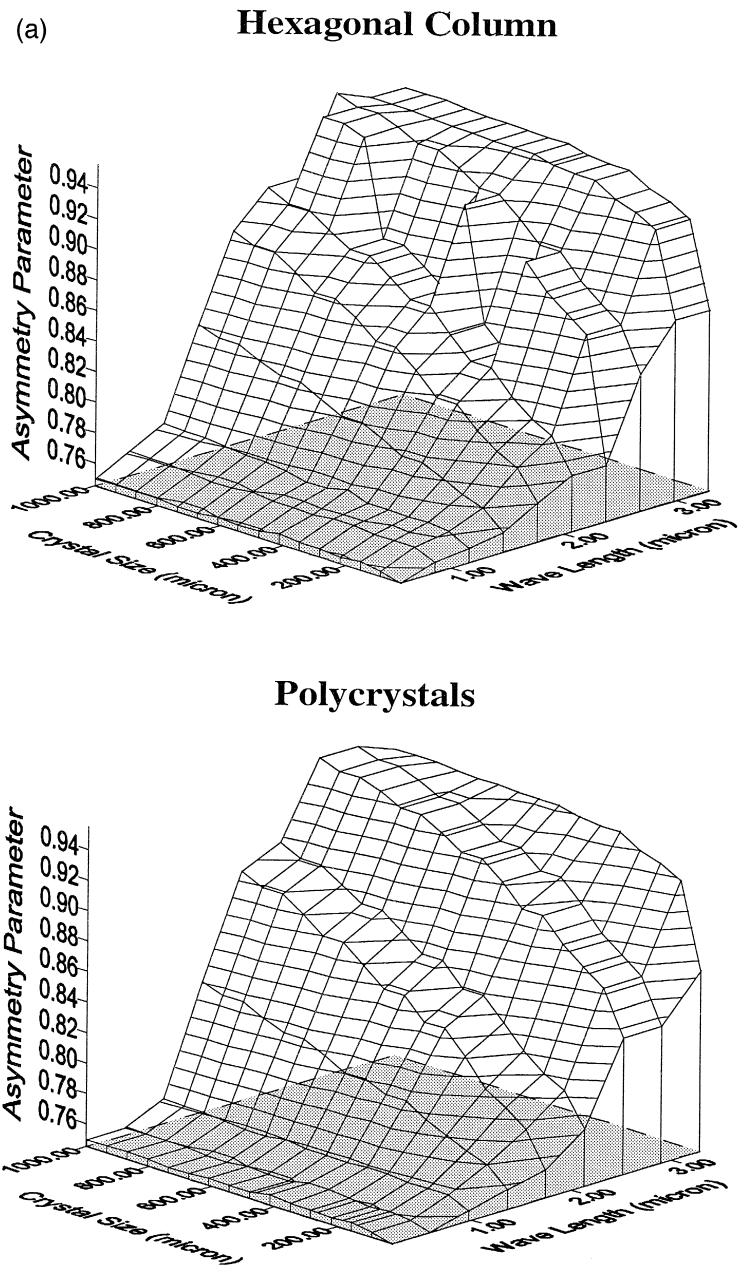

Fig. 3. Asymmetry factor (a) and single scattering albedo (b) as a function of crystal size (in microns) and wavelength (in microns) for hexagonal columns and polycrystals ice particles.

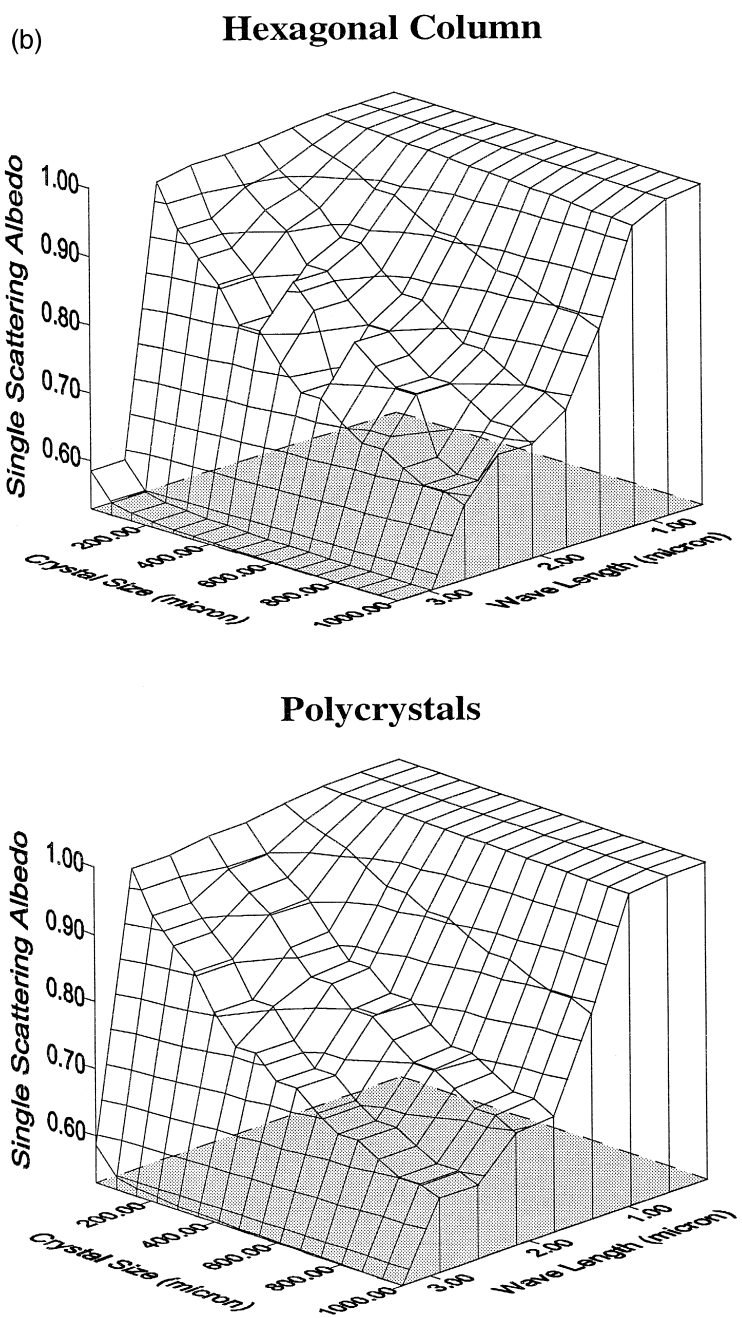

Fig. 3 (continued).

The optical parameters of the nonspherical ice crystals are calculated by a ray-tracing method (Macke et al., 1996). Fig. 3 shows asymmetry factor (a) and single scattering albedo (b) depending on the wavelength and crystal size for hexagonal columns and random polycrystals, which are used as input in the calculation of CRF.

3.1. Small spherical ice particles

Fig. 4 demonstrates how the net cloud radiative forcing (CRF), infrared cloud radiative forcing (ICRF) and solar cloud radiative forcing (SCRF) depend on the mean ice particle size, IWC and cloud thickness of cloud with a single-modal crystal size distribution. ICRF is positive, i.e., it exhibits a cloud greenhouse effect, while SCRF is negative, i.e., it exhibits a cloud albedo effect. The values of CRF change significantly with IWC, cloud thickness and the mean particle size. Firstly, values of CRF, ICRF and SCRF increase as IWC and cloud thickness increase. However, as the value of IWC or cloud thickness is doubled, the value of CRF decreases greatly in the smaller crystal size range, but does not change very much in the larger size range, although ICRF and SCRF both show significant changes. Secondly, for a given value of IWC, the values of CRF, ICRF and SCRF can change greatly with changing mean size of the ice crystals. The sign of CRF can change from positive to negative as the mean size of particles decreases. For the case of a 1 km cloud thickness and IWC = 10 mg m^{-3}, this change

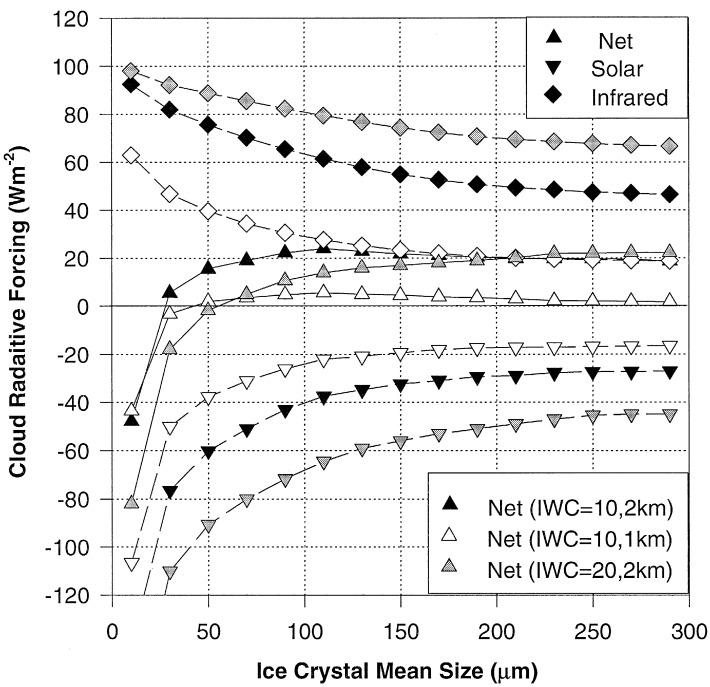

Fig. 4. Cirrus (net, infrared and solar) radiative forcing depending on the crystal mean size, cloud thickness and IWC for single-modal size distribution of crystals.

occurs at a particle size of 30 μm. Fig. 4 shows that the negative CRF in the small size range results from negative SCRF surpassing positive ICRF. Therefore, the negative CRF is caused by the strong albedo effect of small ice particles, which dominates over their greenhouse effect. Thus, cirrus clouds containing relatively large ice particles can produce the 'greenhouse warming' in the Earth–atmosphere. However, for thin clouds containing small particles, the values of CRF would be negative, which means that this kind of cirrus can produce a 'cooling effect' in the Earth–atmosphere.

For a fixed IWC of 10 mg m^{-3}, the mean size of ice particles is about 30 μm assuming that the particle concentration is about 10^7 m^{-3}. Such a high ice crystal concentration rarely occurs in natural cirrus clouds, except in contrail-induced cirrus clouds (Rangno and Hobbs, 1983; Gayet et al., 1996; Kaercher et al., 1996). Therefore, for thin contrail-induced cirrus clouds consisting of single-modal ice particle size spectra, high ice particle concentrations and very small quasi-spherically shaped ice particles, the values of CRF might be negative. This suggests that the contrail-induced cirrus clouds might have a cooling effect instead of a greenhouse warming effect on the climate, which is thought to be the case for natural cirrus clouds. The cooling potential of contrail cirrus as obtained by this investigation agrees with and confirms the suggestion made by Sassen (1997).

In the small size range, not only the values of CRF, but also the solar albedo at the top of the atmosphere, the albedo difference from the clear-sky atmosphere ($\Delta ALB = ALB_{cloud} - ALB_{clear}$), and the infrared upward emittance at cloud top and downward emittance at cloud bottom change dramatically. Fig. 5 shows the dependence of these cloud radiative parameters on the mean size of the crystal size distributions, the shape of the crystal size distributions and the particle shape. Fig. 5 demonstrates the essential changes in the cloud solar albedo and infrared emittance within the small size range of the mean ice particle (10–50 μm) for 10 mg m^{-3} of IWC. For instance, cloud albedo varies from 0.609 to 0.351 and the albedo difference ΔALB from 0.413 to 0.177 for the 2-km cloud thickness case, as the mean size of ice crystal increases from 10 μm to 50 μm.

3.2. Pattern of ice crystal size spectrum

Bi-modal size spectra of ice particles were frequently measured during ICE, EUCREX and FIRE. Based on the information drawn from these field measurements, the bi-modal size spectra for a fixed IWC of 10 mg m^{-3} were simulated (shown in Fig. 2) with the method described in Section 2 and used as input for the CRF estimation. Fig. 6 shows the radiative forcing of clouds with simulated single- and bi-modal crystal size spectra. It is noticed that CRF for the bi-modal case is smaller than that for the single-modal case, although the values of IWC for the bi-modal spectra are the same as those for the single-modal spectra. A possible explanation would be that there are more small crystals at the expense of large ice crystals in the bi-modal case. Furthermore, the percentage (P_{sm}) of small ice particles (smaller than 100 μm) in the total particle concentration is examined. In Fig. 7, P_{sm} for single- and bi-modal cases are compared. As expected, P_{sm} is higher in the smaller mean size range for both single- and bi-modal cases. For the bi-modal case, it is also higher in the larger mean size range. Obviously,

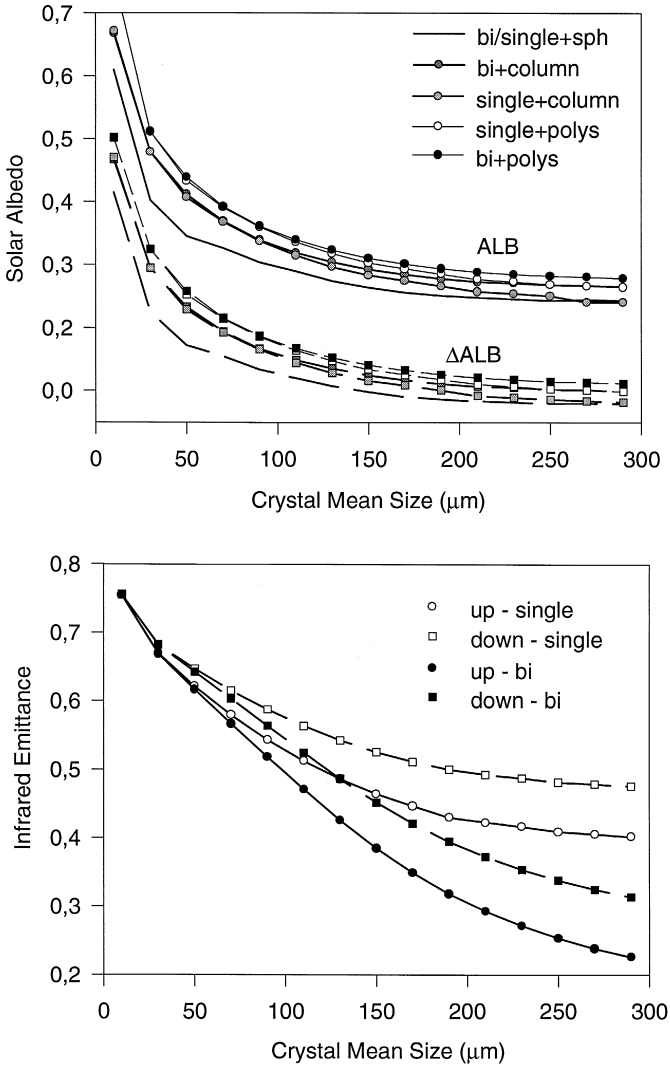

Fig. 5. Cirrus solar albedo (upper) and up- and down-infrared emittance (lower) as a function of mean crystal size for single- and bi-modal size distributions and for different crystal shapes (sphere, hexagonal column and polycrystals). (IWC = 10 mg m^{-3}).

P_{sm} is almost 100% for the particle size at the second peak (second maximum size) in both spectrum cases smaller than 30 μm. While P_{sm} decreases with increasing mean size in the single-modal case, it decreases to a minimum of 56% at about 130 μm then increases to a maximum of 85% at 290 μm for the bi-modal spectrum case. Therefore, it is the smaller crystals with stronger reflective properties that have a dominating influence on the cloud radiative forcing in the bi-modal case. It is also notable that the changing trend in P_{sm} is exactly opposite to that in CRF. The value of the radiative

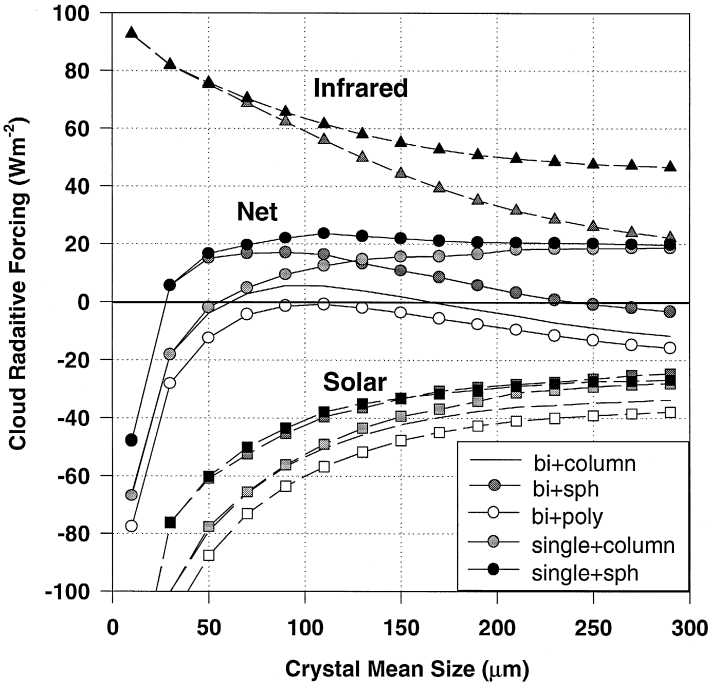

Fig. 6. Cirrus (net, infrared and solar) radiative forcing depending on the crystal mean size, the crystal shape and pattern of size spectrum for 10 mg m^{-3} of IWC and 2 km of cloud thickness.

forcing of a cloud with a bi-modal particle size spectrum first increases then decreases, as the particle size at the second peak moves from the smaller to the larger end. For the

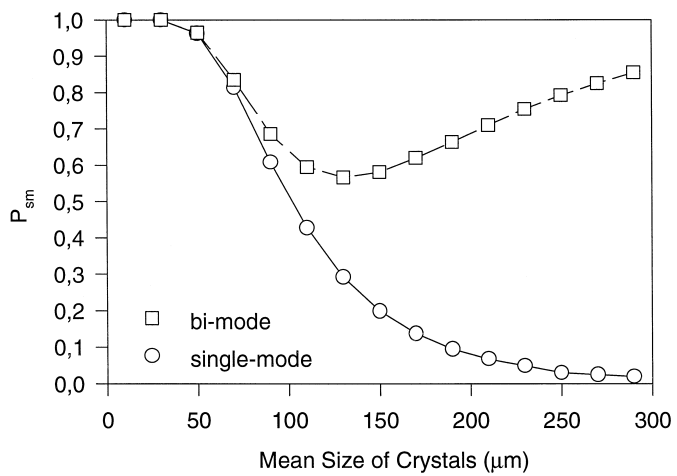

Fig. 7. Percentage of ice crystals smaller than 100 μm (P_{sm}) in crystal concentration for single- and bi-modal size spectra depending on crystal size.

single-modal size distribution case, the decrease in P_{sm} from smaller to larger sizes is similarly opposite to the trend in CRF.

3.3. Nonspherically shaped ice crystals

Fig. 6 demonstrates the differences in CRF between cirrus clouds composed of equivalent spherical and nonspherical ice crystals (hexagonal columns and random polycrystals), together with the differences in CRF between cirrus with bi-modal and single-modal patterns of ice crystal size spectra. The values of IWC for all cases are fixed to 10 mg m^{-3}. Obviously, solar CRF depends essentially on the shape of the ice crystals. The solar radiative forcing of clouds composed of nonspherical ice crystals is much lower than that of clouds composed of surface equivalent spherical crystals, due to higher reflective properties of nonspherical particles in the solar spectral range. Furthermore, the decrease in cirrus solar radiative forcing due to the random polycrystal shape of crystals is even larger than that due to the hexagonal column shape, because polycrystals are more reflective than columns.

For a bi-modal size spectrum and nonspherical crystals, the albedo effect is even more pronounced. For columns, net CRF decreases and turns to negative values as the second maximum size r_{m2} exceeds 170 μm. For random polycrystals with bi-modal size spectra, negative values of net CRF are found for all values of r_{m2}.

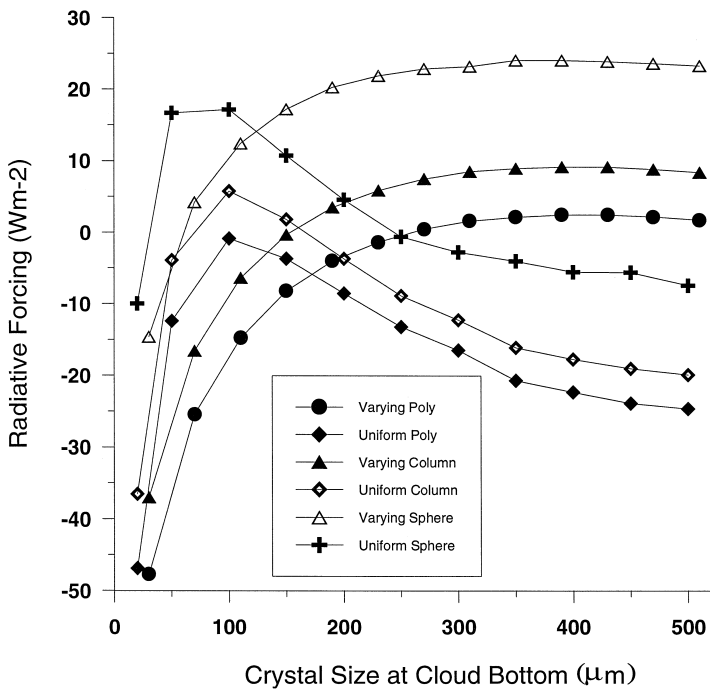

Fig. 8. Cirrus net radiative forcing of clouds with vertically varying or uniform crystal size spectra for various crystal types.

3.4. Vertically varying crystal size distribution

To investigate the effect of vertical variation of crystal size spectrum (see Fig. 1), the net cloud radiative forcing was estimated for the following cases. All cases are for the same value (10 mg m^{-3}) of IWC. First, vertically uniform crystal size spectra from cloud top to bottom for the three crystal types. Second, vertically varying crystal size spectra with the second maximum size drifting linearly from 10 μm at cloud top to a larger size (30–510 μm) at cloud bottom. Obviously, the pattern of the crystal size spectrum at the cloud top tends to be single-mode. Fig. 8 demonstrates the net cloud radiative forcing for the various cases. In general, the size-dependence of radiative forcing of the clouds with vertically varying spectra differs substantially from that of clouds with vertically uniform crystal size spectra. The former increases at small mean particle size then changes little until to large mean particle size, whereas the latter increases sharply and turns to decrease at small mean sizes (about 100 μm). For cloud bottom with a second maximum size larger than 180 μm, the cloud radiative forcing for vertically varying spectra cases is overall higher than that in uniform spectra cases. Therefore, the radiative forcing of natural clouds would be higher than that estimated for idealized clouds with vertical uniform crystal size spectra given the same microphysical situation (same crystal type, IWC, etc.).

4. Discussion and conclusions

In the present work, the sensitivities of cloud radiative forcing as well as solar albedo and infrared emittances to the pattern of cirrus crystal size spectra and to the crystal types were examined with a coupled cloud microphysics and radiation model. The following are the main results.

- Cirrus cloud radiative forcing, which reflects the potential climate impact of cirrus, is extremely sensitive to crystal shape and to crystal size distribution.
- It was found that normal natural cirrus clouds with single-modal crystal size distribution and with relative large ice crystals produce positive cloud radiative forcing, i.e., the potential impact of greenhouse warming on the Earth–atmosphere system. However, for contrail-induced cirrus with extreme microphysical features (i.e., with large numbers of very small ice particles), the cloud radiative forcing would be negative. These contrail-induced cirrus clouds have a potential cooling effect on the Earth–atmosphere system.
- Compared to a single-modal size distribution of ice crystals with the same IWC, it was found that cirrus clouds with bi-modal size distribution of ice crystals tend to have a smaller warming effect, or even a cooling effect, when the size at the second maximum of bi-modal particle size spectrum is relatively large.
- Cloud radiative forcing strongly depends on the ice crystal shape (in this work, hexagonal column and random polycrystals). Since nonspherical ice particles have larger albedo effects, the net radiative forcing of a cloud containing nonspherical ice crystals is much lower than that of a cloud with spherical particles. When the size at the second maximum of bi-modal crystal size spectrum r_{m2} is relatively large (e.g., r_{m2} is larger

than 170 μm for 10 mg m^{-3} of IWC), the net radiative forcing of a cloud with hexagonal column-shaped ice particles is negative. Moreover, for random polycrystals with bi-modal size spectra, the radiative forcing is negative at all values of r_{m2}.

· The radiative forcing of natural clouds would be higher than that estimated for idealized clouds with vertical uniform crystal size spectrum at the same microphysical situation (same crystal type, IWC, etc.).

According to the results mentioned above, cirrus CRF is very sensitive to small ice crystals, the shape of ice crystals and the pattern of ice particle size distribution, suggestions and further comments are made as follows.

· The results shown above imply that CRF depends sensitively not only on IWC and cloud thickness, but also on ice crystal shape and parameters related to the prognostic crystal size distribution. The parameterization involving only IWC and cloud thickness in GCMs is merely a first-order approximation in modeling cirrus cloud–climate interactions. To minimize the errors in the simulation of cloud impacts on the climate, more detailed features of cloud crystal size distribution and nonspherical crystal shapes should be considered as variables in the modeling.

· As known from field-measured results, cirrus ice particle size distributions vary spatially and temporally with cloud type and background weather conditions. Therefore, there is not any simple parameterization of cloud crystal size distribution that can be used for better simulation of the clouds. The parameterization describing the combination of various cloud size spectrum features in cloud–climate modeling must be established with the parameters mentioned above. To reach the goal of a better climate simulation, more measured data are needed to identify suitable sets of cloud microphysical features for improving the cloud parameterization.

· More advanced instruments are also essential and need to be developed for better detecting small crystals in cirrus, which have very important radiative characteristics.

Acknowledgements

The authors appreciate the suggestions and comments given by reviewers and the editor during revision of the manuscript. This work at GKSS was supported by BMBF Project No. V53001.

References

Albers, F., 1991. Improvement for the analysis of 2D probe data. International Cirrus Experiment/European Cloud Radiation Experiment, Fourth Workshop, Reading, UK.

Arnott, W.P., Dong, Y.Y., Hallett, J., 1994. Role of small ice crystals in radiative properties of cirrus: a case study, FIRE II, November 22, 1991. J. Geophys. Res. 99, 1371–1381.

Fischer, G., 1989. Numerical data and functional relationships in science and technology, sub b: Meteorology, Vol. 4. Springer-Verlag, 570 pp.

Gayet, J.F., Febvre, G., Brogniez, G., Chepfer, H., Renger, W., Wendling, P., 1996. Microphysical and optical properties of cirrus and contrails: cloud field study on 13 October 1989. J. Atmos. Sci. 53, 126–138.

Heymsfield, A.J., 1975. Cirrus uncinus generating cells and the evolution of cirriform clouds. Part I: Aircraft observations of the growth of the ice phase. J. Atmos. Sci. 32, 799–808.

Heymsfield, A.J., Platt, C.M.R., 1984. A parameterization of the particle size spectrum of ice clouds in terms of the ambient temperature and the ice water content. J. Atmos. Sci. 41, 846–855.

Kaercher, B., Peter, Th., Biermann, U.M., Schumann, U., 1996. The initial composition of jet condensation trails. J. Atmos. Sci. 53, 3066–3083.

Kerschgens, M., Pilz, U., Raschke, E., 1978. A modified two-stream approximation for computations of the solar radiation budget in a cloudy atmosphere. Tellus 30, 429–435.

Kinne, S., Liou, K.-N., 1989. The effects of the nonsphericity and size distribution of ice crystals on the radiative properties of cirrus clouds. Atmos. Res. 24, 273–284.

Knollenberg, R.G., Dascher, A.J., Huffman, D., 1982. Measurements of the aerosol and ice crystal populations in tropical stratospheric cumulonimbus anvils. Geophys. Res. Lett. 9, 613–616.

Koch, W., 1996. Solarer Strahlungstransport in Arktischem Cirrus. PhD Thesis. GKSS 96/E/60, 99 pp.

Macke, A., 1993. Scattering of light by polyhedral ice crystals. Appl. Opt. 32, 2780–2788.

Macke, A., Mueller, J., Raschke, E., 1996. Single scattering properties of atmospheric ice crystals. J. Atmos. Sci. 53, 2813–2825.

Macke, A., Francis, P.N., McFarquhar, G.M., Kinne, S., 1998. The role of ice particle shapes and size distributions in the single scattering properties of cirrus clouds. J. Atmos. Sci. 55, 2874–2883.

Mishchenko, M.I., Rossow, W.B., Macke, A., Lacis, A.A., 1996. Sensitivity of cirrus cloud albedo, bidirectional reflectance and optical thickness retrieval accuracy to ice particle shape. J. Geophys. Res. 101, 16973–16985.

Mitchell, D.L., Chai, S.K., Liu, Y., Heymsfield, A.J., Dong, Y., 1996. Modeling cirrus clouds. Part I: Treatment of bimodal size spectra and case study analysis. J. Atmos. Sci. 53, 2952–2966.

Ramaswamy, V., Detwiler, A., 1986. Interdependence of radiation and microphysics in cirrus clouds. J. Atmos. Sci. 43, 2289–2301.

Rangno, A.L., Hobbs, P.V., 1983. Production of ice particles in clouds due to aircraft penetrations. J. Clim. Appl. Meteorol. 22, 214–232.

Rockwitz, K.-D., 1989. Scattering properties of horizontally oriented ice crystal columns in cirrus clouds. Appl. Opt. 28, 4103–4111, Part 1.

Sassen, K., 1997. Contrail-cirrus and their potential for regional climate changes. Bull. Am. Meteor. Soc. 78, 1885–1903.

Schmetz, J., 1984. On the parameterization of the radiative properties of broken clouds. Tellus 36, 417–432.

Schmetz, J., Raschke, E., 1981. An approximate computation of infrared radiative fluxes in a cloudy atmosphere. Pure Appl. Geophys. 119, 248–258.

Stenchikov, G.L., Kirchner, I., Robock, A., Graf, H.-F., Antuna, J.C., Grainger, R., Lambert, A., Thomason, L., 1997. Radiative Forcing from the 1991 Mount Pinatubo Volcanic Eruption. Max-Planck-Institut fuer Meteorologie, Rep. No. 231, 40 pp.

Stephens, G.L., Tsay, S.-C., Stackhouse, P.W. Jr., Flatau, P.J., 1990. The relevance of the microphysical and radiative properties of cirrus clouds to climate and climate feedback. J. Atmos. Sci. 47, 1742–1753.

Wendling, P., Wendling, R., Weickmann, H.K., 1979. Scattering of solar radiation by hexagonal ice crystals. Appl. Opt. 18, 2663–2671.

Zhang, Y., Laube, M., Raschke, E., 1989. Numerical studies of the time behaviour of cirrus in still air. Contrib. Atmos. Phys. 62, 307–320.

Zhang, Y., Laube, M., Raschke, E., 1992. Evolution of stratiform cirrus simulated in a lifting layer. Contrib. Atmos. Phys. 65, 23–34.

Zhang, Y., Laube, M., Raschke, E., 1994. Numerical simulation of cirrus properties. Contrib. Atmos. Phys. 67, 109–120.